LANGMUIR

pubs.acs.org/Langmuir Article

Interfacial Self-Assembly of Antimicrobial Peptide GL13K into Non-Fibril Crystalline β-Sheets

Hala Youssef and Christine E. DeWolf*

Cite This: *Langmuir* 2020, 36, 660−665 Read Online

ACCESS | Metrics & More | Article Recommendations | Supporting Information

ABSTRACT: The need for new and potent antibiotics in an era of increasing multidrug resistance in bacteria has driven the search for new antimicrobial agents, including the design of synthetic antimicrobial peptides (AMPs). While a number of β-sheet forming AMPs have been proposed, their similarity to β-amyloids raises a number of concerns associated with neurodegenerative states. GL13K is an effective, synthetic AMP that selectively folds into β-sheets at anionic interfaces. Moreover, it is one of relatively few AMPs that preferentially fold into β-sheets without bridging disulfides. The interfacial activity of GL13K and its propensity to form amyloid fibrils have not been investigated. Using structural studies at the air/water interface and in the absence of anionic lipids, we demonstrate that while GL13K does form crystalline β-sheets, it does not self-assemble into fibrils. This work emphasizes the requirement for a single charged amino acid in the hydrophobic face to prevent fibril formation in synthetic peptides.

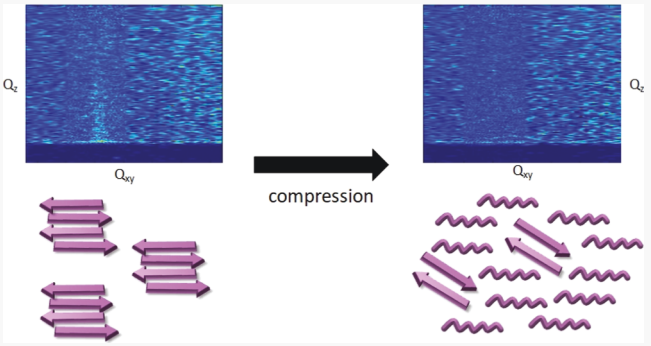

INTRODUCTION

Antibiotic resistance in bacteria has driven the search for new antimicrobial agents, including the design of synthetic antimicrobial peptides (AMPs) whose functionality can be optimized to improve their bactericidal capabilities. While the majority of AMPs preferentially fold into amphipathic α-helices and subsequently induce membrane disruption and cell death, there is a smaller subsection of AMPs that fold preferentially into β-sheets, for example, arenicin-1, protegrin-1, tachyplesin, gramicidin S, defensin, and labaditin.[1−6] For the most part, these AMPs depend on disulfides to maintain their secondary structures and bactericidal activities.[7−9]

GL13K is a synthetic thirteen-residue, cationic AMP that effectively kills both Gram-positive and Gram-negative bacteria.[10−12] It has a net positive charge of +5 at physiological pH, and biophysical characterization showed that the peptide preferentially folds into β-sheets in the presence of anionic bilayers but remains unstructured in buffer and in the presence of zwitterionic membranes.[13] NMR studies showed that GL13K has a propensity to fold into α-helices in zwitterionic micelles but confirmed the preferential folding into β-sheets in anionic bicelles.[14]

β-sheet forming amyloids have been linked to numerous neurodegenerative diseases including Parkinson's disease, Alzheimer's disease, spongiform encephalopathies (mad cow disease), and type II diabetes.[15] While there are no distinct sequence similarities between amyloid β (Aβ) peptides, prion proteins and islet amyloid polypeptide (IAPP), all three form the characteristic cross-β structure.[16] It has been proposed that there is a functional link between AMPs and amyloids in that they both disrupt cell membranes and induce cell death.[17] Despite their different sequences and properties, some AMPs have been shown to form cross-β structures, for example, protegrin-1 was found to undergo amyloidosis and form fibrils with much faster kinetics than Aβ 1−42,[18] implying a potential risk in using β-sheet forming AMPs as antimicrobial agents. Previous studies showed that GL13K formed twisted fibrils when stored in buffers of pH greater than 9 for extended periods[19] and, similarly, deprotonation of the amino-terminus has been shown to drive fibril formation in pentapeptides.[20]

Peptide self-association at the air/water interface has been employed for scaffold formation for templated biomineralization,[21−23] in food processing applications,[24] and to design supramolecular assemblies and nanostructured surfaces.[21,25,26] Moreover, the air/water interface has been proposed as a model hydrophobic interface analogous to the membrane aqueous surface.[23] Compression of peptide and protein monolayers has been used to probe the different stages of protein folding[24,27] and to mimic the macromolecular crowding conditions of different cell compartments.[24] Studying peptide self-association at the air/water interface (in the

Received: October 7, 2019
Revised: December 15, 2019
Published: December 27, 2019

https://dx.doi.org/10.1021/acs.langmuir.9b03120
Langmuir 2020, 36, 660−665

absence of lipids) has been highlighted as an essential first step to understanding their membranes.[28−30]

Adopting the approach employed for the study of peptides, including Aβ peptides, NK2, and arenicin,[28,29,31,32] we have investigated GL13K organization at the air/water interface to ascertain whether the GL13K folds at the air/water interface in the absence of a membrane, and if so, whether it preferentially folds into β-sheets and whether these sheets are aggregated into fibrils.

MATERIALS AND METHODS

Materials. Sodium phosphate monobasic monohydrate ($NaH_2PO_4·H_2O$) and sodium phosphate dibasic heptahydrate ($Na_2HPO_4·7H_2O$) salts purchased from Sigma-Aldrich and Fischer Scientific, respectively, were of purity >98%. All experiments were conducted using 10 mM sodium phosphate buffer that was adjusted to pH 7.4. GL13K (sequence GKIIKLKASLKLL-NH2) was purchased from BioBasic Inc. (ON, Canada) with a purity of >95%. No further purification was conducted. Stock peptide solutions of 1−2 mg/mL were prepared by dissolving the peptide in ultrapure water (18.2 MΩ cm^{-1}) obtained from a Barnstead Easypure II purification system. This water was used to prepare all buffer and peptide solutions.

Surface Pressure−Area Isotherms. Surface pressure−area isotherms were obtained using a NIMA Langmuir film balance with a surface area of 80 cm^2. 6 μL of peptide was spread from a 1.2 mg/mL solution on the surface of 10 mM sodium phosphate (pH 7.4) buffer and allowed to equilibrate at the interface for 30 min prior to compression. The film was compressed at a speed of 5 cm^2/min using mobile barriers. Surface pressure−area isotherms were measured at least 5 times to ensure reproducibility of the peptide film. All experiments were conducted at room temperature.

Grazing Incidence X-ray Diffraction and X-ray Reflectivity. Grazing incidence X-ray diffraction (GIXD) and X-ray reflectivity (XR) experiments were conducted at the NSF's ChemMatCARS beamline 15 ID-C at Argonne National Laboratory (Lemonte, IL, USA). Experiments were conducted using a 340 cm^2 NIMA Langmuir film balance and the same experimental procedure was followed with the exception of the compression speed which was increased to 10 cm^2/min given the larger surface area of this trough. The trough was sealed in a chamber and then flushed with water-saturated helium to reduce scattering by oxygen in the air.

The parameters of the X-ray beams were: wavelength 1.239 Å, incidence angle 0.09061°, and horizontal and vertical sizes 20 and 120 μm, respectively, producing a beam footprint of 20 μm by 7.6 cm. The X-rays were diffracted from the air/water interface, and the diffracted intensity was monitored using a 2D Swiss Light source PILATUS 100K detector set to single-photon counting mode. Two sets of slits, one placed in front of the detector and the other placed 280.0 mm from the sample, were used to minimize intense low-angle scattering. Data were patched using software developed by Wei Bu, a beamline scientist at ChemMatCARS. The in-plane Bragg peaks in the GIXD data were fit using Lorentzian functions using OriginLab Graphing and Analysis software. The position and full width at half maximum of these peaks were used to determine the *d*-spacing and correlation lengths, respectively, as has been described previously.[33]

For XR measurements,[34,35] the reflectivity intensities at Q_z angles ranging between 0.01 and 0.7 $Å^{-1}$ were measured. These intensities were then normalized by the Fresnel reflectivity and analyzed using ChemMatCARS software developed by Wei Bu to generate an electron density profile. The slab model was used to fit the normalized reflectivity data and generate an electron density profile. This electron density profile is an average over the footprint of the beam and represents the vertical distribution of electron density in the film. Starting electron densities were estimated based on values in the literature followed by optimization to improve the fit.

Polarization Modulation Infrared Reflection Absorption Spectroscopy. Polarization modulation infrared reflection absorption spectroscopy (PM-IRRAS) experiments were conducted at Université Laval (Québec City, QC, CA) on an instrument that has been described in detail by Bourque et al.,[36] a home-built Langmuir film balance of surface area 180 cm^2 and 5 mm depth coupled with a NIMA pressure sensor. Infrared light from a Nicolet iS50 Fourier transform IR spectrophotometer (Thermo Scientific, Madison, WI) was reflected off the air/water interface at a grazing angle and measured using a photovoltaic MCT detector (Kolmar Technologies, Newburyport, MA). The polarization of the beam was modulated with a photoelastic modulator PEM-90 (Hinds Instruments, Hillsboro, OR) that was set for optimum efficiency at 1600 cm^{-1}.

Spectra were generated by the co-addition of 1024 scans that were recorded at a scanning mirror velocity of 0.47 cm/s and a resolution of 8 cm^{-1}. Normalized spectra were obtained by plotting the difference of the spectra of the covered and bare subphase divided by the spectra of the bare subphase. OMNIC software was used to process the spectra and correct the baselines. PM-IRRAS selection rules state that transition dipoles that are parallel with the surface will produce positive bands, whereas transition dipoles that are oriented perpendicular to the interface will yield negative bands.[37] Spectra of α-helices and β-sheets were compared to simulations by Blaudez et al. to determine the orientation of peptides at the interfaces.[38]

Atomic Force Microscopy. Atomic force microscopy (AFM) imaging was performed on peptide films transferred onto a mica substrate from the air/water interface via the Langmuir−Blodgett (LB) deposition method.[39] By this method, the freshly cleaved mica is submerged in the subphase prior to spreading the peptide. Once the desired surface pressure has been reached, the substrate was pulled out of the subphase at a speed of 1 mm/min while holding the surface pressure constant. Transfers were conducted at surface pressures of 5, 10, 15, 20, and 30 mN/m, and images were collected in air at room temperature.

A Nanoscope IIIa (Digital Instruments, Santa Barbara, CA) was used in tapping mode with etched silicon cantilevers with a tip radius of <10 nm, frequency of ∼300 kHz, nominal spring constant of 20−80 N/m, and scan rate of 1 Hz. An oscillation amplitude of 175 mV and medium damping (∼25%) were employed.

RESULTS AND DISCUSSION

GL13K is extremely surface active on 10 mM sodium phosphate and forms a very stable monolayer (Figure 1).

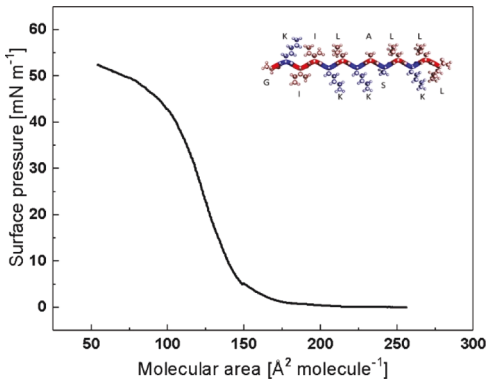

Figure 1. Schematic representation of the sequence of GL13K (inset, hydrophilic and charged residues are blue) and surface pressure−area isotherm of GL13K on a 10 mM sodium phosphate buffer, pH 7.4 subphase.

The critical area, the area at which the peptides begin to interact and form a coherent film, corresponds with the dimensions of a fully extended peptide and indicates that the peptides lie flat at the interface prior to compression. Brewster angle microscopy (BAM) has been used to visualize in situ changes in morphology in response to compression of peptide monolayers.[40,41] With GL13K, the emergence of a coherent

https://dx.doi.org/10.1021/acs.langmuir.9b03120
Langmuir 2020, 36, 660−665

film at higher surface pressures yielded a subtle change in light intensity but no distinct morphological features could be distinguished (data not shown). Thus, if peptide aggregates are present, they must be below the resolution of BAM (<1 μm).

Vertical electron density profiles and lateral organization were derived from X-ray scattering methods. The electron density profiles (Figure 2) were generated using a two-slab

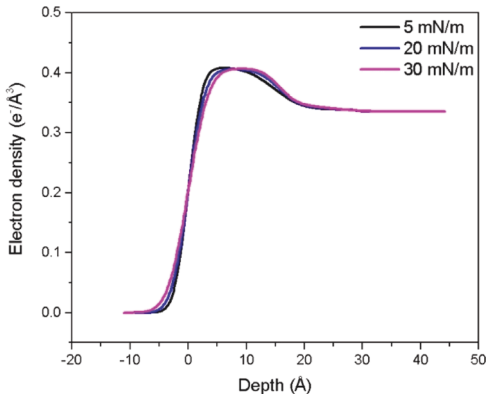

Figure 2. Fitted electron density profiles for GL13K at the air/buffer interface at 5, 20, and 30 mN/m.

model by fitting the normalized XR data (Table S1). The second slab was added to improve the quality of the fit and account for the contribution of adsorbed ions and structured water.[42] It was not possible to fit the data to a simple one-slab model. There does not appear to be significant vertical reorganization at the air/water interface as the GL13K film is compressed. The electron density profiles imply that there is a single layer of peptides at the interface with a diffuse layer of ions directly underneath. The latter likely results from the high charge density of the peptide. The electron density and roughness of the second layer decrease with increasing surface pressure indicating that the ion layer becomes less diffuse attributed to a higher surface charge density as the peptides become closer-packed.

While XR provides information about vertical organization at the interface, GIXD provides information about lateral organization. Peptides that organize into crystalline β-sheets have been shown to exhibit a peak at Q_{xy} ~1.3 and 0.1−0.2 Å^{-1}, corresponding to the inter-strand spacing due to hydrogen bonding and the repeat distance (end-to-end) between the peptides along the backbone axis, respectively.[26,32,43,44]

The GIXD intensity (integrated over Q_z) as a function of Q_{xy} for GL13K is shown in Figure 3. A Bragg peak is observed at the Q_{xy} position 1.32 Å^{-1}, but no peak was observed at lower Q_{xy}. This shows that the peptide organizes into crystalline β-sheets at surface pressures as low as 5 mN/m, but this crystallinity is one-directional given the absence of the low Q_{xy} peak. The crystallinity at 5 and 20 mN/m, given by the correlation length (Supporting Information, Table S2), is similar to that observed for Aβ 40 but significantly weaker than that of the short, 12-residue amyloid-like peptide LSFD for which a coherence length greater than 500 Å was observed.[45] As the film is compressed to small surface areas, the crystallinity of the peptide peak weakens from a length corresponding to ~6 peptides to the point of being negligible at a surface pressure of 30 mN/m. In all cases, the peaks remain at or near Q_z = 0 Å^{-1}, showing that the β-sheets are not significantly bent or twisted at the interface.[26]

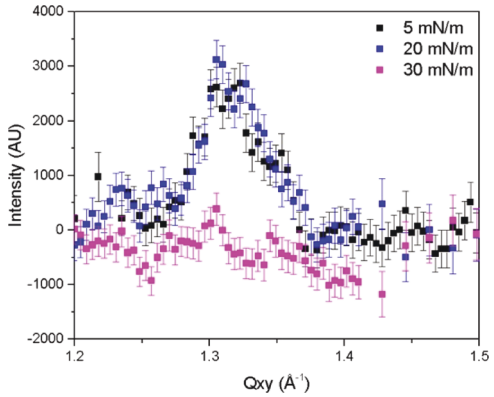

Figure 3. Bragg peak profiles as a function of the in-plane scattering vector component Q_{xy} for GL13K at the air/buffer interface at surface pressures of 5, 20, and 30 mN/m.

To ensure that the method of formation of the film does not alter the peptide organization, GIXD measurements were performed and compared for spread monolayers and adsorbed monolayers, the latter from both dilute solution and after injection of a concentrated stock into the subphase. All three methodologies yield the same Bragg peak, a lack of Bragg peaks at low Q_{xy}, and similar electron density profiles (Supporting Information, Tables S1 and S2).

While GIXD demonstrates a loss of β-sheet crystallinity, it does not indicate the overall secondary structure of the peptide at the interface. PM-IRRAS provides information about ordered secondary structures as well as their orientation at the air/water interface.[38] Figure 4 shows the PM-IRRA spectra

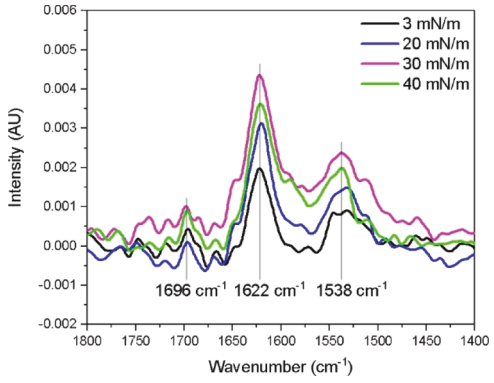

Figure 4. PM-IRRA spectra for GL13K at the air/buffer interface at surface pressures of 5, 20, 30, and 40 mN/m.

for GL13K spread at the interface. At all surface pressures, the amide I band position is ~1620 cm^{-1}. Typically, amide I bands of β-sheets are at positions closer to 1630 cm^{-1}; however, the band position can shift to as low as 1619 cm^{-1} with an increasing number of strands.[46] This supports the GIXD results indicating that GL13K forms an extended β-sheet network, not just single β-strands. A weak second amide I band at 1696 cm^{-1} and the amide II band at 1538 cm^{-1} are also assigned to β-sheet formation. The ratio of the intensities of the main amide I and amide II bands can be used to determine the orientation of the peptide. By comparison to simulated data for interfacial β-sheets,[38] it can be seen that the peptide does not lie completely flat at the interface and becomes more tilted with compression. The angle of the long axis of the peptide relative to the normal of the interface (denoted as θ by

https://dx.doi.org/10.1021/acs.langmuir.9b03120
Langmuir 2020, 36, 660−665

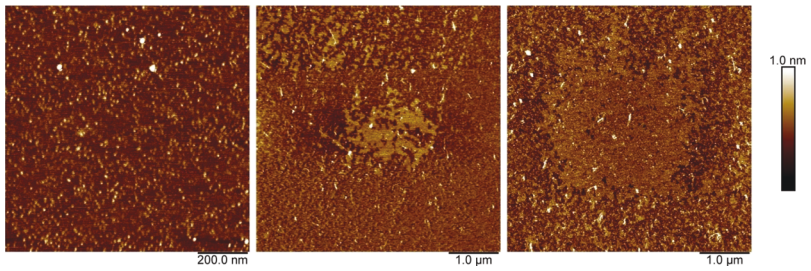

Figure 5. AFM images of GL13K deposited on mica from the air/buffer interface at surface pressures of 15 (a), 20 (b), and 30 mN/m (c). Note that (a) is a 1 μm scan while (b,c) are 5 μm scans.

Blaudez et al.) is ∼90°, that is, parallel to the interface; however the angle of the carbonyls relative to the interface (Ψ) is between 0 and 45°. Compression of the film causes the axes of the peptide to become more tilted, that is θ to become smaller and Ψ to become 45°. At 20 mN/m, θ is ∼70°, and at 30 and 40 mN/m, θ is ∼50°. This increase in the tilt angle would explain the slight increase in thickness of the peptide monolayer observed by XR (Supporting Information, Table S1).

To determine if fibrils were forming at the interface, despite the low crystallinity, AFM was conducted on transferred peptide films (Figure 5). At surface pressures of 15 mN/m and below, small non-fibril agglomerations (bright spots) with heights ∼0.2−0.4 nm above the background can be observed (Figure 5a). AFM studies of other peptide monolayers have reported heights of ∼0.7−1.4 nm[47−49] for lying down β-sheets depending on the sequence, while end-on β-sheets exhibited heights of about 3 nm,[49] but this is a function of peptide length. Our height differences are significantly lower which we have attributed to the co-existence of unstructured and β-sheet peptides. The agglomerations resemble the structures observed by Ye et al. after GL13K was incubated for 8 days at pH 9.4.[19] At higher surface pressures, we observe the appearance of larger domains coexisting with the small domains although, notably, the height difference remains the same; presumably only the proportions of unstructured and β-sheet peptides are changed. In contrast, Shin et al. observed an increase in larger (higher) amorphous agglomerations with increasing surface pressure for films of synthetic polypeptides, which they attributed to surface micelle structures[50] that appear to form because of the block copolymer nature of their peptide. The larger domains appear more prominently in the transfers conducted at both 20 and 30 mN/m (Figure 5b,c). However, the size of these domains does not appear to correlate with the surface pressure as both large domains and regions devoid of such large domains can be observed at both 20 and 30 mN/m (see Figure S2 for additional AFM images). Although the domains can grow to sizes nominally greater than the lateral resolution of BAM, these were not observed because of the high density of smaller domains in the surrounding matrix, such that there is insufficient contrast in the optical properties between the phases. The height difference between the domain and the background matrix suggests a co-existence between ordered β-sheets and random coil peptides. Although the thickness of the β-sheet regions is comparable to that observed for the amyloid-like peptide LSFD deposited onto the solid substrate, there is no evidence of the regular, close-packed fibrils observed for this peptide.[41]

This surface organization of GL13K is in agreement with both experimental and computational findings that the propensity to form β-sheets does not necessarily imply fibril formation.[51,52] Computational studies with eight-residue peptides of varying sequences found a hydrophobic−polar−hydrophobic (HPH) sequence motif was important for the formation of β-sheets.[52] Amyloid fibril formation, which is driven by specific Coulombic interactions and hydrophobic interactions, is dependent on a nucleation seed.[31,53,54] For example, the side-chains often form an interdigitated steric zipper motif[16] for which an Ile > Leu mutation has been shown to prevent fibril formation by disruption of the close-contact face of the peptides.[51]

Multiple variables have been suggested as contributors to amyloidosis. Increasing the net positive charge of the peptide has been shown to lower peptide self-association even when the hydrophobic face of amphipathic peptides is unaltered as this produces a peptide that has a lower net hydrophobicity.[55] There is evidence that peptide length may also contribute because biomimetic β3R3-peptides ranging from 8 to 17 β-amino acids exhibited a loss of crystallinity and inter-peptide networking with increased length.[44] It has also been suggested that the presence of a lysine on the non-polar face prevents peptide self-association in solution with α-helical peptides, thereby increasing their activity by increasing the partitioning to the membrane, as long as the secondary structure remains amphipathic.[55] A similar mechanism can prevent self-association of β-sheets into fibrils. All of these factors apply to GL13K and explain why it does not form fibrils. On the other hand, while protegrin-1 has a net charge of +7 and has arginine residues on its hydrophobic face (PDB 1PG1), it does form fibrils. Notably, protegrin-1 adopts an internal β-hairpin conformation held by two disulfide bridges; thus despite its longer sequence it actually forms shorter β-sheets.

CONCLUSIONS

GL13K is an AMP that assembles preferentially into crystalline antiparallel β-sheets. GL13K did not form fibrils at pH 7.4, despite reports of fibril formation at higher pH. It is thought that fibril formation is likely prevented by GL13K's net charge of +5 and the lysine on its hydrophobic face. This leads to the conclusion that deprotonation of the lysine that lies on the hydrophobic face, which should have a lower pK_a than the amino-terminus, thus drives the hydrophobic interactions required for fibril formation at higher pH. For therapeutic applications, this residue must remain protonated to prevent amyloid behaviour. At high surface pressures, the peptides continue to exhibit β-sheet behaviour but lose crystallinity, and this loss of crystallinity appears to be driven by a compression-induced increase in peptide tilt. Understanding how interfacial crowding impacts β-sheet crystallinity is an essential first step

https://dx.doi.org/10.1021/acs.langmuir.9b03120
Langmuir 2020, 36, 660−665

towards understanding how different membrane environments may affect peptide association and activity.

■ ASSOCIATED CONTENT

Supporting Information

The Supporting Information is available free of charge at https://pubs.acs.org/doi/10.1021/acs.langmuir.9b03120.

GIXD and XR data and fits; additional AFM images (PDF)

■ AUTHOR INFORMATION

Corresponding Author

Christine E. DeWolf − *Concordia University, Montreal, Canada;* orcid.org/0000-0002-5185-7237; Email: christine.dewolf@concordia.ca

Other Author

Hala Youssef − *Concordia University, Montreal, Canada*

Complete contact information is available at: https://pubs.acs.org/10.1021/acs.langmuir.9b03120

Author Contributions

The manuscript was written through contributions of all the authors. All the authors have given approval to the final version of the manuscript.

Funding

The authors acknowledge the financial support from the Natural Sciences and Engineering Research Council (NSERC, grant number 03977-2014) of Canada and the Canada Foundation for Innovation (CFI, grant number 8071).

Notes

The authors declare no competing financial interest.

■ ACKNOWLEDGMENTS

We wish to thank Christian Salesse for useful discussions of PM-IRRAS data analysis and interpretation. The NSF's ChemMatCARS Sector 15 is supported by the Divisions of Chemistry (CHE) and Materials Research (DMR), National Science Foundation, under grant number NSF/CHE-1834750. Use of the Advanced Photon Source, an Office of Science User Facility operated for the U.S. Department of Energy (DOE) Office of Science by Argonne National Laboratory, was supported by the U.S. DOE under contract no. DE-AC02-06CH11357.

■ ABBREVIATIONS

Aβ, amyloid β; AMP, antimicrobial peptide; BAM, Brewster angle microscopy; GIXD, grazing incidence X-ray diffraction; HPH, hydrophobic−polar−hydrophobic; IAPP, islet amyloid polypeptide; LB, Langmuir−Blodgett; PM-IRRAS, polarization modulation infrared reflection absorption spectroscopy

■ REFERENCES

(1) Andrä, J.; Jakovkin, I.; Grötzinger, J.; Hecht, O.; Krasnosdembskaya, A. D.; Goldmann, T.; Gutsmann, T.; Leippe, M. *Biochem. J.* **2008**, *410*, 113−122.

(2) Mani, R.; Waring, A. J.; Lehrer, R. I.; Hong, M. *Biochim. Biophys. Acta, Biomembr.* **2005**, *1716*, 11−18.

(3) Kawano, K.; Yoneya, T.; Miyata, T.; Yoshikawa, K.; Tokunaga, F.; Terada, Y.; Iwanaga, S. *J. Biol. Chem.* **1990**, *265*, 15365−15367.

(4) Ashrafuzzaman, M.; Andersen, O. S.; McElhaney, R. N. *Biochim. Biophys. Acta, Biomembr.* **2008**, *1778*, 2814−2822.

(5) Trabi, M.; Schirra, H. J.; Craik, D. J. *Biochemistry* **2001**, *40*, 4211−4221.

(6) Barbosa, S. C.; Cilli, E. M.; Dias, L. G.; Stabeli, R. G.; Ciancaglini, P. *Amino Acids* **2011**, *40*, 135−144.

(7) Zhang, X.-J.; Zhang, X.-Y.; Zhang, N.; Guo, X.; Peng, K.-S.; Wu, H.; Lu, L.-F.; Wu, N.; Chen, D.-D.; Li, S.; Nie, P.; Zhang, Y.-A. *J. Immunol.* **2015**, *194*, 4974−4987.

(8) Fázio, M. A.; Oliveira, V. X.; Bulet, P.; Miranda, M. T. M.; Daffre, S.; Miranda, A. *Biopolymers* **2006**, *84*, 205−218.

(9) Mohanram, H.; Bhattacharjya, S. *Biochim. Biophys. Acta, Gen. Subj.* **2014**, *1840*, 3006−3016.

(10) Abdolhosseini, M.; Nandula, S. R.; Song, J.; Hirt, H.; Gorr, S.-U. *Peptides* **2012**, *35*, 231−238.

(11) Hirt, H.; Gorr, S.-U. *Antimicrob. Agents Chemother.* **2013**, *57*, 4903−4910.

(12) Chen, N.; Li, J.; Li, D.; Yang, Y.; He, D. *PLoS One* **2014**, *9*, No. e113453.

(13) Balhara, V.; Schmidt, R.; Gorr, S.-U.; DeWolf, C. *Biochim. Biophys. Acta, Biomembr.* **2013**, *1828*, 2193−2203.

(14) Harmouche, N.; Aisenbrey, C.; Porcelli, F.; Xia, Y.; Nelson, S. E. D.; Chen, X.; Raya, J.; Vermeer, L.; Aparicio, C.; Veglia, G.; Gorr, S.-U.; Bechinger, B. *Biochemistry* **2017**, *56*, 4269−4278.

(15) Qiang, W.; Yau, W.-M.; Schulte, J. *Biochim. Biophys. Acta, Biomembr.* **2015**, *1848*, 266−276.

(16) Eisenberg, D.; Jucker, M. *Cell* **2012**, *148*, 1188−1203.

(17) Zhang, M.; Zhao, J.; Zheng, J. *Soft Matter* **2014**, *10*, 7425−7451.

(18) Jang, H.; Arce, F. T.; Mustata, M.; Ramachandran, S.; Capone, R.; Nussinov, R.; Lal, R. *Biophys. J.* **2011**, *100*, 1775−1783.

(19) Ye, Z.; Zhu, X.; Acosta, S.; Kumar, D.; Sang, T.; Aparicio, C. *Nanoscale* **2019**, *11*, 266−275.

(20) Do, T. D.; LaPointe, N. E.; Economou, N. J.; Buratto, S. K.; Feinstein, S. C.; Shea, J.-E.; Bowers, M. T. *J. Phys. Chem. B* **2013**, *117*, 10759−10768.

(21) Cavalli, S.; Handgraaf, J.-W.; Tellers, E. E.; Popescu, D. C.; Overhand, M.; Kjaer, K.; Vaiser, V.; Sommerdijk, N. A. J. M.; Rapaport, H.; Kros, A. *J. Am. Chem. Soc.* **2006**, *128*, 13959−13966.

(22) Segman-Magidovich, S.; Rapaport, H. *J. Phys. Chem. B* **2012**, *116*, 11197−11204.

(23) Jain, A.; Jochum, M.; Peter, C. *Langmuir* **2014**, *30*, 15486−15495.

(24) Banc, A.; Desbat, B.; Renard, D.; Popineau, Y.; Mangavel, C.; Navailles, L. *Langmuir* **2007**, *23*, 13066−13075.

(25) Tanaka, M.; Ogura, K.; Abiko, S.; Koshikawa, N.; Kinoshita, T. *Polym. J.* **2008**, *40*, 1191−1194.

(26) Vaiser, V.; Rapaport, H. *J. Phys. Chem. B* **2011**, *115*, 50−56.

(27) Small, D. M.; Wang, L.; Mitsche, M. A. *J. Lipid Res.* **2009**, *50*, S329−S334.

(28) Olak, C.; Muenter, A.; Andrä, J.; Brezesinski, G. *J. Pept. Sci.* **2008**, *14*, 510−517.

(29) Travkova, O. G.; Andrä, J.; Möhwald, H.; Brezesinski, G. *ChemPhysChem* **2010**, *11*, 3262−3268.

(30) Ambroggio, E. E.; Fidelio, G. D. *Biochim. Biophys. Acta, Biomembr.* **2013**, *1828*, 708−714.

(31) Thakur, G.; Micic, M.; Leblanc, R. M. *Colloids Surf., B* **2009**, *74*, 436−456.

(32) Chi, E. Y.; Frey, S. L.; Winans, A.; Lam, K. L. H.; Kjaer, K.; Majewski, J.; Lee, K. Y. C. *Biophys. J.* **2010**, *98*, 2299−2308.

(33) Jensen, T. R.; Kjaer, K. In *Novel Methods to Study Interfacial Layers*; Mobius, D., Miller, R., Eds.; Elsevier B.V: Amsterdam, 2001; Vol. *11*, pp 205−254.

(34) Behyan, S.; Borozenko, O.; Khan, A.; Faral, M.; Badia, A.; DeWolf, C. *Environ. Sci.: Nano* **2018**, *5*, 1218−1230.

(35) Bu, W.; Mihaylov, M.; Amoanu, D.; Lin, B.; Meron, M.; Kuzmenko, I.; Soderholm, L.; Schlossman, M. L. *J. Phys. Chem. B* **2014**, *118*, 12486−12500.

(36) Bourque, H.; Laurin, I.; Pézolet, M.; Klass, J. M.; Lennox, R. B.; Brown, G. R. *Langmuir* **2001**, *17*, 5842−5849.

(37) Blaudez, D.; Turlet, J.-M.; Dufourcq, J.; Bard, D.; Buffeteau, T.; Desbat, B. *J. Chem. Soc., Faraday Trans.* **1996**, *92*, 525−530.
(38) Blaudez, D.; Castano, S.; Desbat, B. In *Biointerface Characterization by Advanced IR Spectroscopy*; Elsevier, 2011; pp 27−55.
(39) Motschmann, H.; Helmuth, M. In *Handbook of Applied Surface and Colloid Chemistry*; Wiley, 2001; pp 629−648.
(40) Leon, L.; Logrippo, P.; Tu, R. *Biophys. J.* **2010**, *99*, 2888−2895.
(41) Lepère, M.; Chevallard, C.; Hernandez, J.-F.; Mitraki, A.; Guenoun, P. *Langmuir* **2007**, *23*, 8150−8155.
(42) Lavoie, H.; Blaudez, D.; Vaknin, D.; Desbat, B.; Ocko, B. M.; Salesse, C. *Biophys. J.* **2002**, *83*, 3558−3569.
(43) Rubinov, B.; Wagner, N.; Rapaport, H.; Ashkenasy, G. *Angew. Chem., Int. Ed.* **2009**, *48*, 6683−6686.
(44) Mosca, S.; Dannehl, C.; Möginger, U.; Brezesinski, G.; Hartmann, L. *Org. Biomol. Chem.* **2013**, *11*, 5399−5403.
(45) Lepère, M.; Muenter, A. H.; Chevallard, C.; Guenoun, P.; Brezesinski, G. *Colloids Surf., A* **2007**, *303*, 73−78.
(46) Barth, A. *Biochim. Biophys. Acta, Bioenerg.* **2007**, *1767*, 1073−1101.
(47) Kowalewski, T.; Holtzman, D. M. *Proc. Natl. Acad. Sci. U.S.A.* **1999**, *96*, 3688−3693.
(48) Jeong, J. S.; Ansaloni, A.; Mezzenga, R.; Lashuel, H. A.; Dietler, G. *J. Mol. Biol.* **2013**, *425*, 1765−1781.
(49) Paribok, I. V.; Kim, Y.-O.; Choi, S. K.; Jung, B. Y.; Lee, J.; Nam, K. T.; Agabekov, V. E.; Lee, Y.-S. *ACS Omega* **2018**, *3*, 3901−3907.
(50) Shin, S.; Ahn, S.; Cheng, J.; Chang, H.; Jung, D.-H.; Hyun, J. *Appl. Surf. Sci.* **2016**, *388*, 551−556.
(51) Lopez de la Paz, M.; Goldie, K.; Zurdo, J.; Lacroix, E.; Dobson, C. M.; Hoenger, A.; Serrano, L. *Proc. Natl. Acad. Sci. U.S.A.* **2002**, *99*, 16052−16057.
(52) Hung, N. B.; Le, D.-M.; Hoang, T. X. *J. Chem. Phys.* **2017**, *147*, 105102.
(53) Murphy, M. P.; LeVine, H., III *J. Alzheimer's Dis.* **2010**, *19*, 311.
(54) Goedert, M. *Science* **2015**, *349*, 1255555.
(55) Jiang, Z.; Vasil, A. I.; Hale, J. D.; Hancock, R. E. W.; Vasil, M. L.; Hodges, R. S. *Biopolymers* **2008**, *90*, 369−383.

https://dx.doi.org/10.1021/acs.langmuir.9b03120
Langmuir 2020, 36, 660−665